Linda M. Nguyen,[1] Marina Pozzoli,[1] Thomas H. Hraha,[1] and Richard K.P. Benninger[1,2]

CrossMark

Decreasing Cx36 Gap Junction Coupling Compensates for Overactive K_{ATP} Channels to Restore Insulin Secretion and Prevent Hyperglycemia in a Mouse Model of Neonatal Diabetes

Mutations to the ATP-sensitive K^+ channel (K_{ATP} channel) that reduce the sensitivity of ATP inhibition cause neonatal diabetes mellitus via suppression of β-cell glucose-stimulated free calcium activity ($[Ca^{2+}]_i$) and insulin secretion. Connexin-36 (Cx36) gap junctions also regulate islet electrical activity; upon knockout of Cx36, β-cells show $[Ca^{2+}]_i$ elevations at basal glucose. We hypothesized that in the presence of overactive ATP-insensitive K_{ATP} channels, a reduction in Cx36 would allow elevations in glucose-stimulated $[Ca^{2+}]_i$ and insulin secretion to improve glucose homeostasis. To test this, we introduced a genetic knockout of Cx36 into mice that express ATP-insensitive K_{ATP} channels and measured glucose homeostasis and islet metabolic, electrical, and insulin secretion responses. In the normal presence of Cx36, after expression of ATP-insensitive K_{ATP} channels, blood glucose levels rapidly rose to >500 mg/dL. Islets from these mice showed reduced glucose-stimulated $[Ca^{2+}]_i$ and no insulin secretion. In mice lacking Cx36 after expression of ATP-insensitive K_{ATP} channels, normal glucose levels were maintained. Islets from these mice had near-normal glucose-stimulated $[Ca^{2+}]_i$ and insulin secretion. We therefore demonstrate a novel mechanism by which islet function can be recovered in a monogenic model of diabetes. A reduction of gap junction coupling allows sufficient glucose-stimulated $[Ca^{2+}]_i$ and insulin secretion to prevent the emergence of diabetes.

Glucose-stimulated insulin secretion from β-cells in the islet is regulated via a series of metabolic and electrical events. The ATP-sensitive K^+ channel (K_{ATP} channel) provides a central role in coupling increases in the ATP/ADP ratio after the metabolism of glucose, to membrane depolarization, elevated intracellular free calcium activity ($[Ca^{2+}]_i$), and insulin granule exocytosis (1). The K_{ATP} channel is made up of inward-rectifying K^+ channel Kir6.2 and sulfonylurea receptor 1 (Sur1). In humans,

[1]Department of Bioengineering, University of Colorado, Anschutz Medical Campus, Aurora, CO
[2]Barbara Davis Center for Childhood Diabetes, University of Colorado, Anschutz Medical Campus, Aurora, CO

Corresponding author: Richard K.P. Benninger, richard.benninger@ucdenver.edu.

mutations in the genes encoding Kir6.2 (*KCNJ11*) and Sur1 (*ABCC8*), which reduce the sensitivity of ATP inhibition and lead to overactive K_{ATP} channels (gain-of-function mutations), are the most common cause of neonatal diabetes mellitus (NDM) (2). Transgenic mice that express ATP-insensitive K_{ATP} channels in β-cells can recapitulate the human disease (3–5). These mice exhibit marked hyperglycemia and reduced plasma insulin, and islets from these mice show a suppression of glucose-stimulated $[Ca^{2+}]_i$ and insulin release (4,6). This demonstrates that a reduction of glucose-dependent excitability underlies the development of diabetes caused by K_{ATP} channel mutations. Inhibition of K_{ATP} channels with sulfonylureas can recover elevations in $[Ca^{2+}]_i$ and insulin secretion in islets of these mouse models (3,4,6). As such, sulfonylureas can be applied to treat patients with NDM associated with K_{ATP} channel mutations (7,8). Nevertheless, some mutations render the K_{ATP} channel insensitive to sulfonylureas (7,9,10).

Cellular interactions within the islet have long been known to be important for enhancing the regulation of insulin release (11) and are also important for regulating electrical activity (12). Connexin-36 (Cx36) gap junction channels regulate islet electrical activity by coupling K_{ATP}-regulated membrane depolarization between β-cells of the islet. This synchronizes oscillations in membrane depolarization and $[Ca^{2+}]_i$ at elevated glucose (13,14), leading to a coordination of first-phase insulin release and pulsatile second-phase insulin release (15). Under normal conditions, Cx36 gap junction channels also enhance a suppression of spontaneous elevations in $[Ca^{2+}]_i$ at basal glucose (16,17); upon a knockout of Cx36, elevated $[Ca^{2+}]_i$ is observed at lower glucose levels (14,18). This suppression likely occurs as a result of the long-established presence of β-cell heterogeneity (19), where inexcitable cells in the islet suppress membrane depolarization and $[Ca^{2+}]_i$ in more excitable cells via gap junction coupling (16,18).

Given that Cx36 gap junction channels coordinate K_{ATP}-regulated membrane potential, we hypothesized that their action in suppressing $[Ca^{2+}]_i$ and insulin occurs more generally under conditions of K_{ATP} channel opening. Therefore, similar to their normal action at lower glucose levels, we hypothesized that Cx36 gap junctions would inappropriately enhance the suppression of $[Ca^{2+}]_i$ and insulin secretion at elevated glucose in the presence of overactive ATP-insensitive K_{ATP} channels in NDM. Therefore, we hypothesized that an absence of Cx36 gap junction coupling upon expression of ATP-insensitive K_{ATP} channels would reduce this suppression and lead to spontaneous elevations in $[Ca^{2+}]_i$ at elevated glucose. We anticipated that this $[Ca^{2+}]_i$ elevation would stimulate sufficient insulin release to prevent the severe hyperglycemia that emerges in these animals. However, we anticipated that suppression of $[Ca^{2+}]_i$ and insulin release would be maintained at low glucose levels; in essence, a decrease in Cx36 will left shift the dose response to

compensate for a right shift due to overactive K_{ATP} channels. Here, we tested this by introducing a knockout of Cx36 gap junction channels into a mouse model of NDM that expresses ATP-insensitive K_{ATP} channels in the β-cell under control of an inducible Cre^{ER}-recombinase (3). We tested whether mice with reduced or absent Cx36 gap junction coupling showed an improvement in glucose homeostasis and whether islets from these mice showed a recovery of glucose-stimulated $[Ca^{2+}]_i$ and insulin secretion.

RESEARCH DESIGN AND METHODS

Animal Care

Experiments were performed in compliance with the relevant laws and institutional guidelines and were approved by the University of Colorado Institutional Animal Care and Use Committee. Mice expressing Rosa26-Kir6.2$^{[ΔN30,K185Q]}$ (Kir6.2$^{[ΔN30,K185Q]}$ gain-of-function mutant), Pdx-Cre^{ER} (pancreas-specific inducible Cre), and Cx36$^{-/-}$ (global Cx36 knockout) were generated as described previously (3,20,21) and supplied by collaborating laboratories. β-Cell conditional expression of Kir6.2$^{[K185Q,ΔN30]}$ is achieved through crossing Rosa26-Kir6.2$^{[ΔN30,K185Q]}$ and Pdx-Cre^{ER} mice to excise a loxP-flanked stop codon to drive Kir6.2$^{[K185Q,ΔN30]}$ expression. Green fluorescent protein (GFP) is coexpressed via an internal ribosome entry site. Rosa26-Kir6.2$^{[ΔN30,K185Q]}$ and Pdx-Cre^{ER} mice either had normal gap junction coupling (to generate Cx36$^{+/+}$; Kir6.2$^{[ΔN30,K185Q]}$ mice) or were first separately crossed with Cx36$^{-/-}$ mice to achieve a homozygous deletion and then bred together (to generate Cx36$^{-/-}$; Kir6.2$^{[ΔN30,K185Q]}$ mice). Cx36$^{+/+}$ or Cx36$^{-/-}$ littermate mice lacking Rosa26-Kir6.2$^{[ΔN30,K185Q]}$ and/or Pdx-Cre^{ER} were used as controls. Mice were studied at generation F3–F5. To prevent genetic drift, new breeders were generated by crossing Cx36$^{+/+}$- and Cx36$^{-/-}$-expressing breeders every two to three generations.

In Vivo Measurements

Each experimental group (age-matched Cx36$^{+/+}$; Kir6.2$^{[ΔN30,K185Q]}$ and Cx36$^{-/-}$;Kir6.2$^{[ΔN30,K185Q]}$ with respective littermate Cx36$^{+/+}$ and Cx36$^{-/-}$ controls) received five daily doses of tamoxifen (50 mg/g body weight) at experimental day 1–5. Blood glucose was measured daily as previously performed (3) with a glucometer (Ascensia Contour; Bayer). Plasma insulin was measured at day 29 from blood samples centrifuged at 14 krev/min for 10 min and assayed using mouse ultrasensitive insulin ELISA (Alpco). Glucose tolerance tests were performed at day 30–32. Littermate or age-matched mice were fasted overnight for 16 h and received intraperitoneal injection of 2 g/kg body weight of glucose, and blood glucose was measured on tail vein blood samples preinjection (0 min) and 15, 30, 60, 90, and 120 min post–glucose delivery. Insulin tolerance tests (ITTs) were performed at day 30–32. Littermate

mice were fasted for 6 h and received intraperitoneal injection of 0.75 units/kg body weight of human recombinant insulin (Novolin; Novo Nordisk), and blood glucose was measured on tail vein blood samples preinjection (0 min) and 15, 30, 45, 60, and 90 min postinjection.

Islet Isolation and Insulin Secretion

At day 30–36, islets were isolated from pancreata of each experimental mouse and maintained in islet medium (RPMI medium, 10% fetal bovine serum, 11 mmol/L glucose, 100 units/mL penicillin, 100 μg/mL streptomycin) at 37°C under humidified 5% CO_2 for 24 h. For static insulin secretion measurements, islets (five per column, in duplicate) were preincubated for 60 min at 37°C in Krebs-Ringer buffer (128.8 mmol/L NaCl, 5 mmol/L $NaHCO_3$, 5.8 mmol/L KCl, 1.2 mmol/L KH_2PO_4, 2.5 $CaCl_2$, 1.2 mmol/L $MgSO_4$, 10 mmol/L HEPES, 0.1% BSA, pH 7.4) plus 2 mmol/L glucose and then incubated for 60 min at 37°C in Krebs-Ringer buffer plus different glucose concentrations and/or reagents as indicated. After the incubation period, the medium was removed and insulin concentration assayed using mouse ultrasensitive insulin ELISA. To estimate insulin content, islets were lysed in 1% Triton X-100 and frozen at −20°C overnight.

Microscopy

All isolated islets were imaged using established methods (13), in polydimethylsiloxane microfluidic devices (16), maintained at 37°C, with imaging medium (125 mmol/L NaCl, 5.7 mmol/L KCl, 2.5 mmol/L $CaCl_2$, 1.2 mmol/L $MgCl_2$, 10 mmol/L HEPES, 2 mmol/L glucose, 0.1% BSA, pH 7.4).

To measure $[Ca^{2+}]_i$ response and dynamics, islets were loaded with 4 μmol/L Fura Red-AM (Invitrogen) for 2 h at room temperature and imaged on a Marianas spinning-disk microscope (3I) with a 40× 1.3 NA Plan-Neofluar oil-immersion objective (Zeiss). Images were acquired 10 min after glucose stimulation. Fura Red was imaged using a 488-nm diode laser for excitation and a 580- to 655-nm band-pass emission filter (Semrock). GFP was imaged using a 488-nm diode laser for excitation and a 500- to 550-nm band-pass emission filter. There was no detectable cross-talk between Fura Red and GFP.

To measure $[Ca^{2+}]_i$ concentration, islets were loaded with 2 μmol/L Fura 2-AM for 30 min at room temperature and imaged on an Eclipse-Ti widefield microscope (Nikon) with a 20× 0.75 NA Plan Apo objective. Images were acquired 10 min after glucose stimulation or immediately after KCl stimulation. Fura 2 was imaged sequentially using 340- and 380-nm (±5 nm) Arc-lamp excitation and a 470- to 550-nm band-pass emission filter (Chroma).

To measure NAD(P)H, islets were imaged on an LSM510 microscope (Zeiss), with a 40× 1.2 NA C-Apochromatic water-immersion objective. NAD(P)H autofluorescence was imaged with two-photon excitation using a 710-nm mode-locked Ti:sapphire laser (Coherent) and a 400- to 500-nm band-pass emission filter (Chroma) and nondescanned detector. GFP fluorescence was imaged using a 488-nm Ar^+ laser line for excitation and a 500- to 550-nm band-pass emission filter. Z-stacks of six images were acquired at 2-μm spacing. No GFP fluorescence was detected in the NAD(P)H channel.

To measure mitochondrial membrane potential changes, islets were loaded with 50 nmol/L Rhodamine 123 for 20 min at 37°C and imaged on an LSM510 microscope with a 40× 1.2 NA C-Apochromatic water-immersion objective. Images were acquired 10 min after glucose stimulation. Rhodamine 123 was imaged using a 488-nm Ar^+ laser line for excitation and a 500- to 550-nm band-pass emission filter. Z-stacks of six images were acquired at 2-μm spacing.

Image Analysis

Images collected on the different microscope systems (3I and Zeiss; Nikon) were analyzed offline in Matlab (Mathworks) using established methods (6,18,22). For Fura 2, 340- and 380-nm intensities were averaged across each islet, and the "background" intensity averaged over an unstained islet subtracted. Time-averaged $[Ca^{2+}]_i$ concentration was calibrated from the background-subtracted time-averaged 340-nm/380-nm intensity ratio using the Fura 2 calibration kit (Invitrogen).

NAD(P)H and Rhodamine 123 fluorescence were averaged across each islet, with Z positions corrected for focal drift. The mean NAD(P)H autofluorescence for each experimental group was normalized to the average autofluorescence in $Cx36^{+/+}$ islets at 2 mmol/L. The mean Rhodamine 123 fluorescence of each islet was normalized to the fluorescence at 2 mmol/L glucose.

To estimate the proportion of the islet showing elevations in $[Ca^{2+}]_i$, Fura Red images were first smoothed using a 3 × 3 average filter. The variance (intensity fluctuation) was calculated over the time course of each pixel. A threshold variance was calculated for a silent cell, identified as quiescent at 2 mmol/L glucose, which represents image noise. An active area showing $[Ca^{2+}]_i$ fluctuations was defined as having a variance significantly greater (95% confidence) than the variance of the silent cell.

To determine high-GFP (GFP$^+$) cells, GFP images were first smoothed using a 3 × 3 average filter. A threshold intensity was calculated from the autofluorescence in the GFP channel from control (GFP$^-$) $Cx36^{+/+}$ or $Cx36^{-/-}$ islets. A GFP$^+$ region was identified as having GFP fluorescence greater than the threshold intensity.

RESULTS

Inducible β-cell expression of mutant ATP-insensitive K_{ATP} channel subunit (Kir6.2$^{[\Delta N30,K185Q]}$) forms K_{ATP} channels with mixed mutant and wild-type Kir6.2 (3), which reduces the sensitivity of ATP inhibition. To test whether reduced Cx36 gap junction coupling could recover sufficient elevation in $[Ca^{2+}]_i$ and insulin secretion

in the presence of ATP-insensitive K_{ATP} channels, age-matched Rosa-Kir6.2[ΔN30,K185Q];Pdx-Cre[ER]–expressing mice with normal Cx36 gap junction coupling (Cx36^{+/+};Kir6.2[ΔN30,K185Q]) and Rosa-Kir6.2[ΔN30,K185Q];Pdx-Cre[ER]–expressing mice with a lack of Cx36 gap junction coupling (Cx36^{−/−};Kir6.2[ΔN30,K185Q]) were selected along with littermate control mice (Cx36^{+/+} and Cx36^{−/−}, respectively). Each group of these four mice underwent tamoxifen injections to induce Kir6.2[ΔN30,K185Q] expression and were studied in parallel.

Cx36 Knockout Prevents Hyperglycemia Upon Mutant K_{ATP} Channel Expression

In Cx36^{+/+};Kir6.2[ΔN30,K185Q] mice, after the induction of Kir6.2[ΔN30, K185Q] expression, ad libitum–fed blood

glucose levels rapidly rose to >500 mg/dL compared with littermate Cx36^{+/+} control animals (Fig. 1A). Plasma insulin levels were substantially and significantly diminished in Cx36^{+/+};Kir6.2[ΔN30,K185Q] mice compared with littermate Cx36^{+/+} controls (Fig. 1B). In Cx36^{−/−};Kir6.2[ΔN30,K185Q] mice, which lack β-cell gap junction coupling, after the induction of Kir6.2[ΔN30,K185Q] expression, ad libitum–fed blood glucose levels remained unchanged compared with Cx36^{−/−} littermate control animals (Fig. 1C). Insulin levels were not significantly reduced in Cx36^{−/−};Kir6.2[ΔN30,K185Q] mice compared with littermate Cx36^{−/−} controls (Fig. 1D). At day 30 postinduction, Cx36^{+/+};Kir6.2[ΔN30,K185Q] mice showed substantially greater blood glucose compared with Cx36^{+/+} controls, whereas Cx36^{−/−};Kir6.2[ΔN30,K185Q] showed no
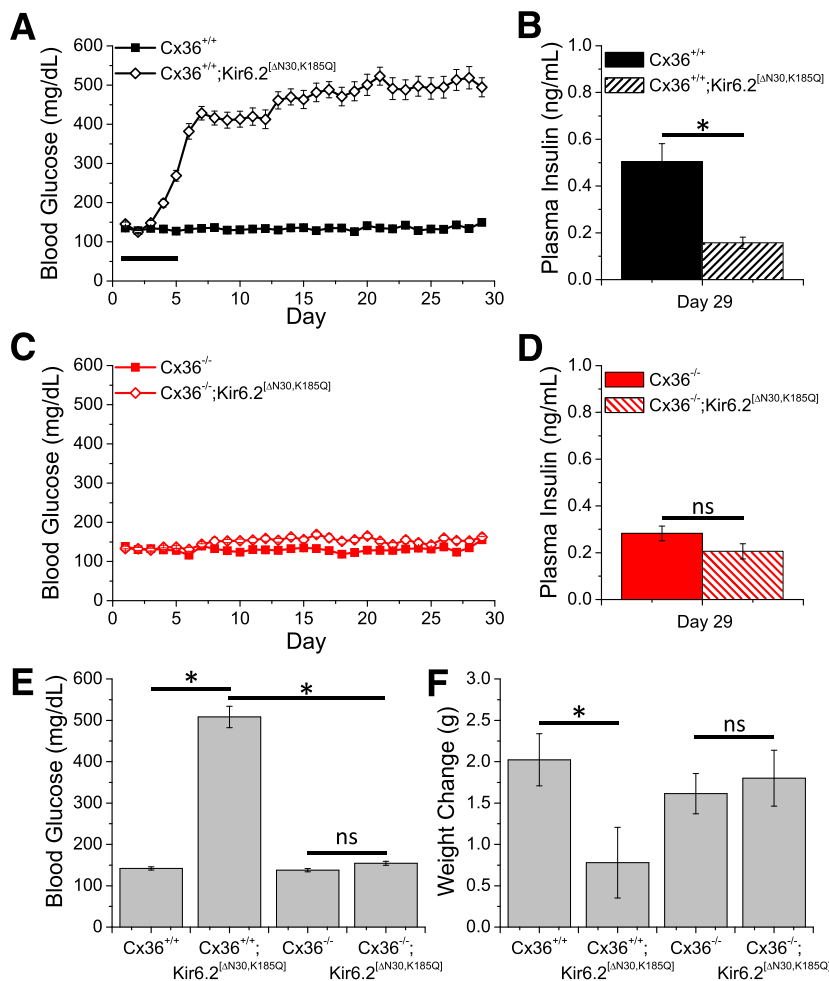
Figure 1—Prevention of Kir6.2[ΔN30,K185Q]-induced hyperglycemia. A: Mean time course of ad libitum–fed blood glucose levels after tamoxifen injection in Cx36^{+/+};Kir6.2[ΔN30,K185Q] mice (open diamond) and control Cx36^{+/+} mice (solid square). Duration of daily tamoxifen injections indicated by solid line. B: Mean plasma insulin levels at day 29 after tamoxifen injection in Cx36^{+/+};Kir6.2[ΔN30,K185Q] mice (hashed bar) and control Cx36^{+/+} mice (solid bar). C: As in A for Cx36^{−/−};Kir6.2[ΔN30,K185Q] mice (open diamond) and control Cx36^{−/−} mice (solid square). D: As in B for Cx36^{−/−};Kir6.2[ΔN30,K185Q] mice (hashed bar) and control Cx36^{−/−} mice (solid bar). E: Mean ad libitum blood glucose levels for all groups of mice, averaged over days 27–29 postinduction. F: Mean weight change for all groups of mice, between days 1 and 29 postinduction. Data in A, C, E, and F averaged over n = 22 (Cx36^{+/+};Kir6.2[ΔN30,K185Q]) and n = 21 (Cx36^{+/+}) littermates. Data in B, D, E, and F averaged over n = 21 (Cx36^{−/−};Kir6.2[ΔN30,K185Q]) and n = 24 (Cx36^{−/−}) littermates. *Significant difference (P < 0.05, two-tailed Student t test); ns, no significant difference (P > 0.05) between each experimental group as indicated. Error bars represent mean ± SEM.

significant increase compared with littermate $Cx36^{-/-}$ controls, and similar to $Cx36^{+/+}$ controls (Fig. 1E). Over the 30 days postinduction, $Cx36^{+/+};Kir6.2^{[\Delta N30,K185Q]}$ mice showed significantly less weight gain compared with $Cx36^{+/+}$ littermate controls, whereas $Cx36^{-/-};Kir6.2^{[\Delta N30,K185Q]}$ showed no significant difference compared with $Cx36^{-/-}$ littermate controls (Fig. 1F).

In $Cx36^{+/-};Kir6.2^{[\Delta N30,K185Q]}$ mice with ~50% gap junction coupling, after the induction of $Kir6.2^{[\Delta N30,K185Q]}$ expression, ad libitum–fed blood glucose levels also rose compared with littermate control animals (Supplementary Fig. 1). This initial elevation was slightly reduced compared with that in $Cx36^{+/+};Kir6.2^{[\Delta N30,K185Q]}$ mice studied in parallel. However, mice ultimately progressed to similar high blood glucose levels >500 mg/dL. Plasma insulin levels were also significantly diminished in $Cx36^{+/-};Kir6.2^{[\Delta N30,K185Q]}$ mice compared with control mice.

$Cx36^{+/+};Kir6.2^{[\Delta N30,K185Q]}$ mice also showed substantially greater fasting blood glucose compared with $Cx36^{+/+}$ controls and poor glucose tolerance during an intraperitoneal glucose tolerance test (IPGTT), as expected given the marked elevation in fed glucose levels (Fig. 2A). Whereas $Cx36^{-/-};Kir6.2^{[\Delta N30,K185Q]}$ mice showed similar fasting blood glucose compared with $Cx36^{-/-}$ controls, they showed significantly elevated glucose levels during an IPGTT, indicating a reduced glucose tolerance (Fig. 2B). During an ITT, $Cx36^{-/-};Kir6.2^{[\Delta N30,K185Q]}$ mice showed only a small elevation in blood glucose levels compared with $Cx36^{-/-}$ controls, indicating a small reduction in insulin sensitivity (Fig. 2C). Therefore, in the presence of Cx36 gap junction coupling, expression of ATP-insensitive K_{ATP} channels results in severe diabetes, whereas in the absence of Cx36 gap junction coupling, only glucose intolerance occurs.

Cx36 Knockout Improves $[Ca^{2+}]_i$ and Insulin Secretion Upon Mutant K_{ATP} Channel Expression

To discover whether the improved glycemic control originated from improvements in stimulus secretion coupling within the islet, we isolated islets from $Cx36^{+/+};Kir6.2^{[\Delta N30,K185Q]}$ and $Cx36^{-/-};Kir6.2^{[\Delta N30,K185Q]}$ mice with their respective littermate controls at 30 days postinduction. Islets isolated from $Cx36^{+/+};Kir6.2^{[\Delta N30,K185Q]}$ and $Cx36^{-/-};Kir6.2^{[\Delta N30,K185Q]}$ mice showed similar levels of GFP coexpression above the level of autofluorescence (Fig. 3A), with on average 50% (each ranging from 30 to 65%) of the islet GFP+ (Fig. 3B). This indicates similar levels of high mutant $Kir6.2^{[\Delta N30,K185Q]}$ expression in each case.

Significantly elevated insulin secretion was observed at elevated glucose levels (20 mmol/L) in islets from $Cx36^{-/-};Kir6.2^{[\Delta N30,K185Q]}$ mice compared with low glucose levels (2 mmol/L), whereas no significant elevation in insulin secretion was observed in islets from $Cx36^{+/+};Kir6.2^{[\Delta N30,K185Q]}$ mice (Fig. 3C). At elevated glucose levels (20 mmol/L), insulin secretion from $Cx36^{+/+};Kir6.2^{[\Delta N30,K185Q]}$ islets was significantly lower compared with $Cx36^{-/-};Kir6.2^{[\Delta N30,K185Q]}$ islets, as well as compared
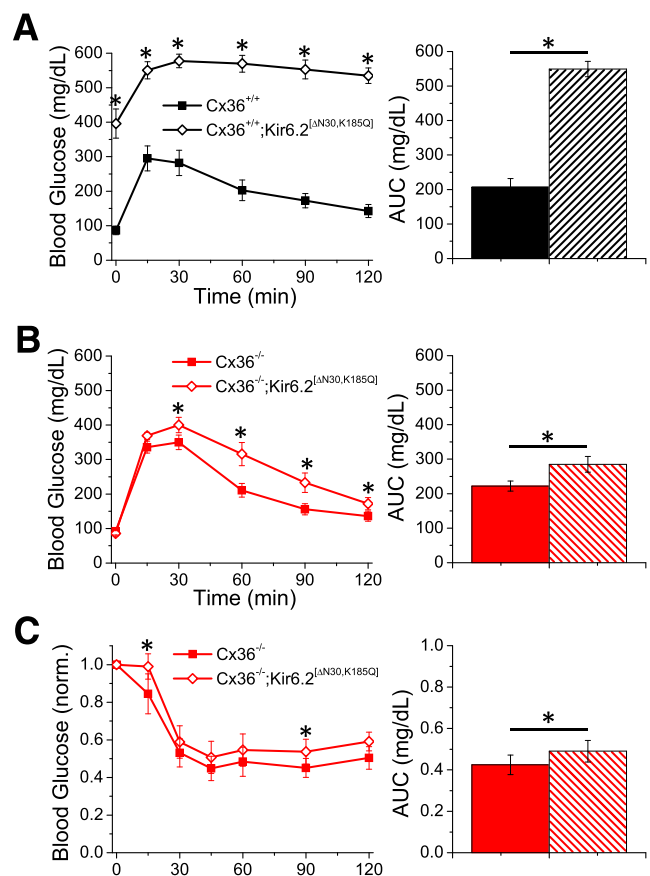
Figure 2—Improved glucose tolerance. *A*: IPGTT on $Cx36^{+/+};Kir6.2^{[\Delta N30,K185Q]}$ mice (open diamond) and control $Cx36^{+/+}$ mice (solid square) after 2 g/kg body weight intraperitoneal glucose injection. *Right*: Area under the curve (AUC) of the glucose excursion. *n* = 6 littermate mice in each group. *B*: As in *A* for $Cx36^{-/-};Kir6.2^{[\Delta N30,K185Q]}$ mice and control $Cx36^{-/-}$ mice. *n* = 11 littermate mice in each group. *C*: ITT for $Cx36^{-/-};Kir6.2^{[\Delta N30,K185Q]}$ mice and control $Cx36^{-/-}$ mice after 0.075 units/kg intraperitoneal insulin injection after 0 time point. *n* = 13 littermate mice in each group. *Significant difference (P < 0.05, two-tailed paired Student *t* test) between each experimental group as indicated. Error bars represent mean ± SEM.

with $Cx36^{+/+}$ and $Cx36^{-/-}$ control islets. Whereas mean glucose-stimulated insulin secretion from $Cx36^{-/-};Kir6.2^{[\Delta N30,K185Q]}$ islets was significantly greater than $Cx36^{+/+};Kir6.2^{[\Delta N30,K185Q]}$ islets, it was ~50% less than $Cx36^{+/+}$ and $Cx36^{-/-}$ control islets. Under elevated KCl stimulation, similar levels of insulin secretion were observed in all cases (Fig. 3C). Insulin content was also slightly reduced in $Cx36^{+/+};Kir6.2^{[\Delta N30,K185Q]}$ islets compared with $Cx36^{+/+}$ controls, whereas similar insulin content was observed in both $Cx36^{-/-};Kir6.2^{[\Delta N30,K185Q]}$ and $Cx36^{-/-}$ islets (Fig. 3D). Therefore, in the absence of Cx36 gap junction coupling, ATP-insensitive K_{ATP} channels have a reduced effect in suppressing glucose-stimulated insulin secretion.

We next examined potential alterations in $[Ca^{2+}]_i$ in islets from these mice. At elevated (11 mmol/L) glucose
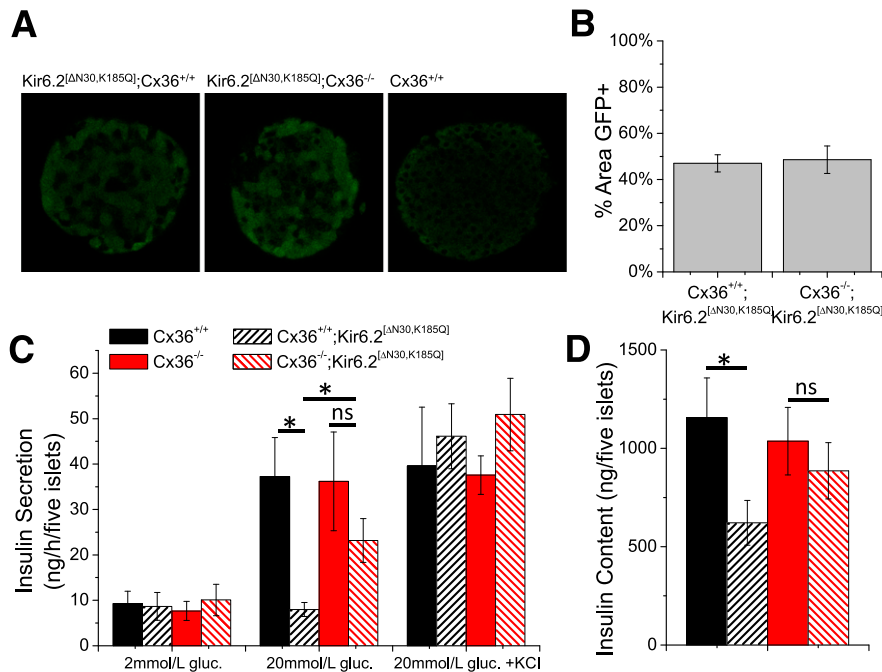
Figure 3—Recovery of glucose-stimulated insulin secretion. A: Representative images of GFP (green) in islets from Cx36$^{+/+}$;Kir6.2$^{[\Delta N30,K185Q]}$, Cx36$^{-/-}$;Kir6.2$^{[\Delta N30,K185Q]}$, and Cx36$^{+/+}$ mice. B: Mean percent coverage of GFP in islets from Cx36$^{+/+}$;Kir6.2$^{[\Delta N30,K185Q]}$ and Cx36$^{-/-}$;Kir6.2$^{[\Delta N30,K185Q]}$ mice. $n = 9$ age-matched mice in each group, two to six islets per mouse. C: Insulin secretion under low glucose (gluc.) (2 mmol/L), high glucose (20 mmol/L), and high glucose plus KCl (+20 mmol/L) in islets isolated from Cx36$^{+/+}$;Kir6.2$^{[\Delta N30,K185Q]}$ and Cx36$^{+/+}$ littermate control mice and Cx36$^{-/-}$;Kir6.2$^{[\Delta N30,K185Q]}$ and Cx36$^{-/-}$ littermate control mice. D: Insulin content in islets isolated from Cx36$^{+/+}$;Kir6.2$^{[\Delta N30,K185Q]}$ and Cx36$^{+/+}$ littermate control mice and Cx36$^{-/-}$;Kir6.2$^{[\Delta N30,K185Q]}$ and Cx36$^{-/-}$ littermate control mice. Data in C and D averaged over $n = 6$ age-matched mice. *Significant difference ($P < 0.05$, two-tailed Student t test); ns, no significant difference ($P > 0.05$) between each experimental group as indicated. Error bars represent mean ± SEM.

levels, transient elevations (oscillations) in [Ca^{2+}]$_i$ were observed in Cx36$^{+/+}$ control islets (Fig. 4A, top). These oscillations were rarely observed in Cx36$^{+/+}$;Kir6.2$^{[\Delta N30,K185Q]}$ islets at elevated glucose levels (Fig. 4A, middle) but observed frequently in many cells of Cx36$^{-/-}$;Kir6.2$^{[\Delta N30,K185Q]}$ islets at elevated (20 mmol/L) glucose (Fig. 4A, bottom). The proportion of cells showing transient elevations in [Ca^{2+}]$_i$ was significantly greater in Cx36$^{-/-}$;Kir6.2$^{[\Delta N30,K185Q]}$ islets compared with Cx36$^{+/+}$;Kir6.2$^{[\Delta N30,K185Q]}$ islets at elevated glucose (Fig. 4B). [Ca^{2+}]$_i$ oscillations were observed at a greater extent in low-GFP$^-$ cells in Cx36$^{-/-}$;Kir6.2$^{[\Delta N30,K185Q]}$ islets compared with high-GFP$^+$ cells (Fig. 4B and Supplementary Fig. 2), and to a similar extent as Cx36$^{+/+}$ control islets. Interestingly, a large proportion of high-GFP$^+$ cells still showed [Ca^{2+}]$_i$ oscillations in Cx36$^{-/-}$;Kir6.2$^{[\Delta N30,K185Q]}$ islets, albeit with a plateau fraction of <10%, compared with between 30 and 90% in low-GFP$^-$ cells (Fig. 4A). Upon elevated glucose levels, the time-averaged free-calcium concentration was also significantly reduced in Cx36$^{+/+}$;Kir6.2$^{[\Delta N30,K185Q]}$ islets compared with Cx36$^{+/+}$ islets (Fig. 4C). At high glucose levels, Cx36$^{-/-}$ islets normally show a reduced time-average free-calcium concentration compared with wild-type islets (18), and no significant difference was observed between Cx36$^{-/-}$; Kir6.2$^{[\Delta N30,K185Q]}$ and Cx36$^{-/-}$ islets. Again, similar

elevations in free-calcium concentration were observed in all groups upon elevated KCl. Therefore, in the absence of Cx36 gap junction coupling, ATP-insensitive K$_{ATP}$ channels have a reduced effect in suppressing glucose-stimulated [Ca^{2+}]$_i$, consistent with the observed recovery of glucose-stimulated insulin secretion.

Cx36 Knockout Improves [Ca^{2+}]$_i$ and Insulin Secretion Upon Diazoxide-Induced K$_{ATP}$ Opening

To further test whether modulating gap junction coupling can enhance [Ca^{2+}]$_i$ and insulin secretion upon K$_{ATP}$ channel opening, this time in the presence of normal β-cell heterogeneity, we applied varying concentrations of the K$_{ATP}$ activator diazoxide. At 11 mmol/L glucose in Cx36$^{+/+}$ islets, 100 μmol/L diazoxide suppressed [Ca^{2+}]$_i$ elevations across most of the islet (Fig. 5A, top), whereas in Cx36$^{-/-}$ islets, many cells still showed [Ca^{2+}]$_i$ elevations (Fig. 5A, bottom). [Ca^{2+}]$_i$ elevations were significantly greater in Cx36$^{-/-}$ islets upon 100 μmol/L diazoxide but not upon 250 μmol/L diazoxide (Fig. 5B). Similarly, upon 100 μmol/L diazoxide at 11 mmol/L glucose, insulin secretion from Cx36$^{-/-}$ islets was significantly greater than Cx36$^{+/+}$ islets. Therefore, in a more general case of K$_{ATP}$ channel opening, a reduction in gap junction coupling elevates [Ca^{2+}]$_i$ and insulin secretion.
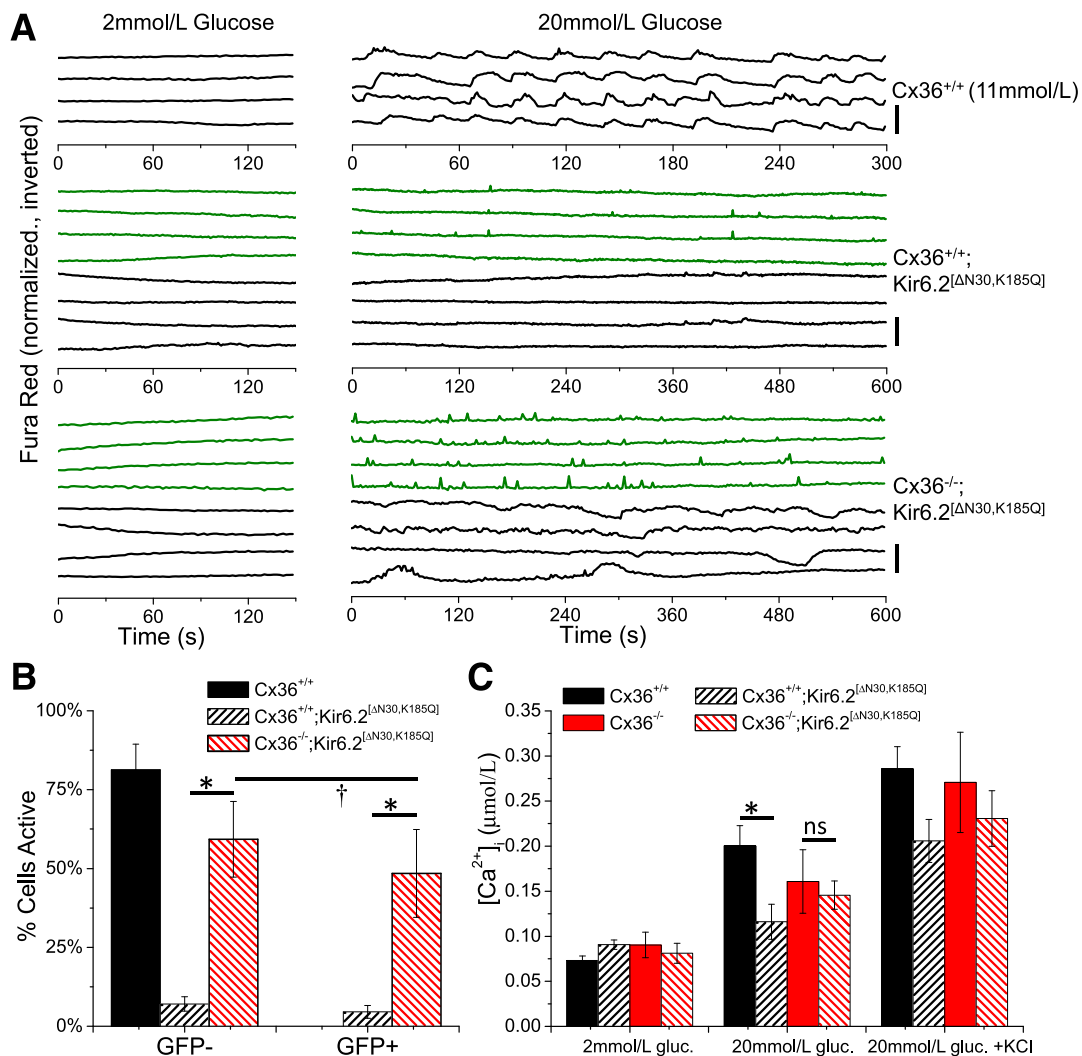
Figure 4—Recovery of glucose-stimulated $[Ca^{2+}]_i$. *A*: Representative time courses of $[Ca^{2+}]_i$, as measured from Fura Red fluorescence, in islets isolated from Cx36$^{+/+}$ mice (*top*), Cx36$^{+/+}$;Kir6.2$^{[\Delta N30,K185Q]}$ mice (*middle*), and Cx36$^{-/-}$;Kir6.2$^{[\Delta N30,K185Q]}$ mice (*bottom*). Displayed is the inverted, normalized Fura Red fluorescence from a number of nonadjacent cells with low GFP expression (black) or high GFP expression (green) at 2 mmol/L glucose (*left*) and 10 min after elevation to 20 mmol/L glucose (*right*), or at 2 and 11 mmol/L glucose in Cx36$^{+/+}$ islets. Time courses are offset for clarity, and vertical scale bar indicates 50% change in Fura Red fluorescence. *B*: Mean percent of cells displaying dynamic changes in $[Ca^{2+}]_i$ at 20 mmol/L glucose in Cx36$^{+/+}$;Kir6.2$^{[\Delta N30,K185Q]}$ islets and Cx36$^{-/-}$;Kir6.2$^{[\Delta N30,K185Q]}$ islets, and at 11 mmol/L glucose in Cx36$^{+/+}$ islets, averaged over high GFP expression only or low GFP expression only. Data averaged over $n = 3$ age-matched mice in each group, three to seven islets per mouse. *C*: Mean $[Ca^{2+}]_i$ concentration measured from Fura 2 fluorescence, under low glucose (gluc.) (2 mmol/L), high glucose (20 mmol/L), and high glucose plus KCl (+20 mmol/L) in islets isolated from Cx36$^{+/+}$; Kir6.2$^{[\Delta N30,K185Q]}$ and Cx36$^{+/+}$ littermate control mice and Cx36$^{-/-}$;Kir6.2$^{[\Delta N30,K185Q]}$ and Cx36$^{-/-}$ littermate control mice. Data averaged over $n = 6$ age-matched mice, two to eight islets per mouse. *Significant difference ($P < 0.05$, two-tailed Student *t* test); †significant difference ($P < 0.05$, two-tailed paired Student *t* test); ns, no significant difference ($P > 0.05$) between each experimental group as indicated. Error bars represent mean ± SEM.

Cx36 Knockout Reduces Metabolic Dysfunction After Mutant K$_{ATP}$ Channel Expression

A secondary consequence of the chronic hyperglycemia and hypoinsulinemia that occurs in Kir6.2$^{[\Delta N30,K185Q]}$-expressing mice is marked mitochondrial dysfunction (6), characterized by reduced mitochondrial NAD(P)H accumulation and reduced mitochondrial membrane depolarization at elevated glucose. We quantified these parameters in mice with reduced gap junction coupling that are protected from diabetes. Cx36$^{+/+}$;Kir6.2$^{[\Delta N30,K185Q]}$

islets showed elevated NAD(P)H at low levels of glucose compared with control Cx36$^{+/+}$ islets, but similar low levels of NAD(P)H were observed in Cx36$^{-/-}$;Kir6.2$^{[\Delta N30,K185Q]}$ islets and control Cx36$^{-/-}$ islets (Fig. 6*A* and *B*). Similar levels of NAD(P)H were observed at elevated glucose in all sets of islets (Fig. 6*A*). As a result, Cx36$^{+/+}$;Kir6.2$^{[\Delta N30,K185Q]}$ islets showed significantly reduced glucose-stimulated accumulation of NAD(P)H compared with other experimental groups (Fig. 6*C*). Cx36$^{+/+}$;Kir6.2$^{[\Delta N30,K185Q]}$ islets also showed significantly reduced mitochondrial membrane
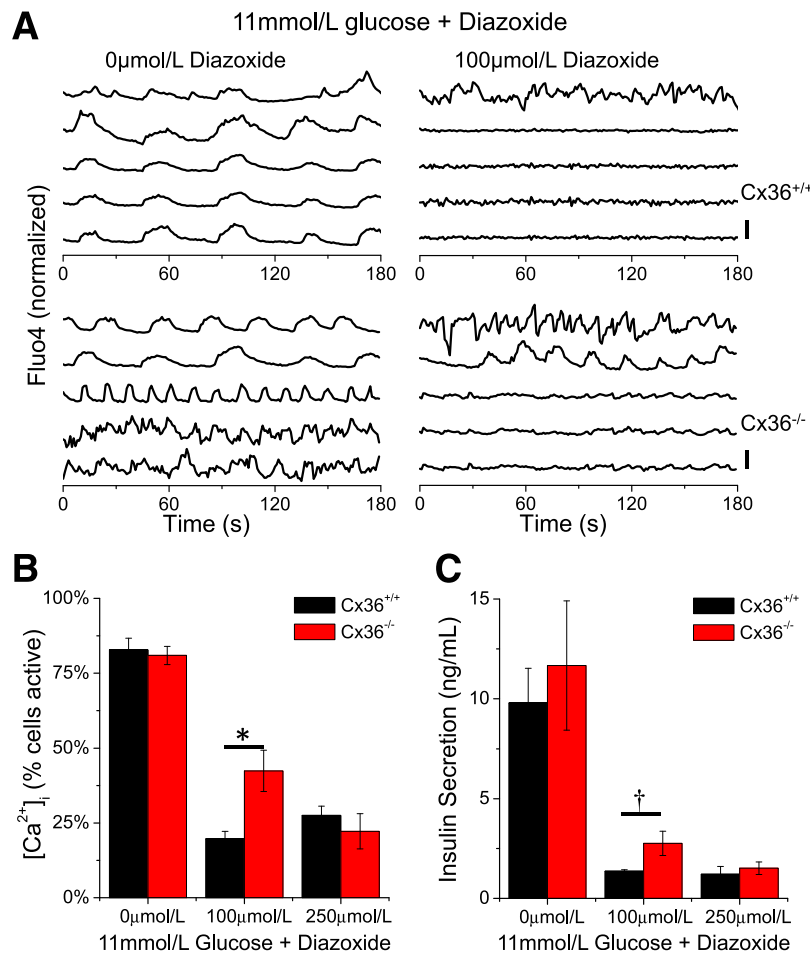
Figure 5—Recovery of $[Ca^{2+}]_i$ in diazoxide-treated islets. *A*: Representative time courses of $[Ca^{2+}]_i$, as measured from Fluo4 fluorescence, in islets isolated from Cx36$^{+/+}$ mice (*top*) and Cx36$^{-/-}$ mice (*bottom*) at 11 mmol/L glucose before and after diazoxide treatment. Displayed is the normalized Fluo4 fluorescence from a number of nonadjacent cells within an islet at 11 mmol/L glucose alone (*left*) and 11 mmol/L glucose 10 min after treatment with 100 μmol/L diazoxide. Time courses are offset for clarity, and vertical scale bar indicates 50% change in Fluo4 fluorescence. *B*: Mean percent of cells displaying dynamic changes in $[Ca^{2+}]_i$ at 11 mmol/L glucose in Cx36$^{+/+}$ and Cx36$^{-/-}$ islets at several diazoxide concentrations. Data averaged over $n = 3$ age-matched mice in each group, two to five islets per mouse. *C*: Insulin secretion under high glucose (11 mmol/L) in Cx36$^{+/+}$ and Cx36$^{-/-}$ islets at several diazoxide concentrations. Data averaged over $n = 6$ age-matched mice in each group. *Significant difference ($P < 0.05$, two-tailed Student *t* test); †significant difference ($P < 0.05$, one-tailed paired Student *t* test). Error bars represent mean ± SEM.

depolarization compared with Cx36$^{-/-}$;Kir6.2$^{[\Delta N30,K185Q]}$ islets at elevated glucose, as indicated by Rhodamine 123 fluorescence (Fig. 6*D–F*). Therefore, reducing gap junction coupling in Kir6.2$^{[\Delta N30,K185Q]}$-expressing mice leads to an absence of secondary mitochondrial dysfunction.

DISCUSSION

In this study, we tested whether a reduction in islet Cx36 gap junction coupling could compensate for overactive ATP-insensitive K$_{ATP}$ channels in a model of NDM, and therefore prevent the emergence of diabetes. Upon a knockout of Cx36, the elevation in glucose-stimulated $[Ca^{2+}]_i$ and insulin secretion that we measured explains the normalization in blood glucose levels. Based on results presented here and prior studies, we propose the following mechanisms of action, schematically

represented in Fig. 7*A*. A reduction in Cx36 gap junctions effectively left shifts the dose response of $[Ca^{2+}]_i$ (although insulin remains suppressed at low glucose due to $[Ca^{2+}]_i$-independent mechanisms of suppression [18]), whereas expression of overactive K$_{ATP}$ channels effectively right shifts the dose response of $[Ca^{2+}]_i$ and insulin secretion (with a largely suppressed response over the physiological glucose range in the presence of Cx36). Therefore, in the presence of overactive K$_{ATP}$ channels, a reduction in Cx36 partially normalized the dose response, albeit with disrupted insulin secretion dynamics associated with a loss of Cx36. This is further detailed in Fig. 7*B*, where in the normal presence of Cx36, inexcitable cells that are present due to heterogeneity prevent membrane depolarization and $[Ca^{2+}]_i$ elevations in normally excitable cells at elevated glucose, via a gap
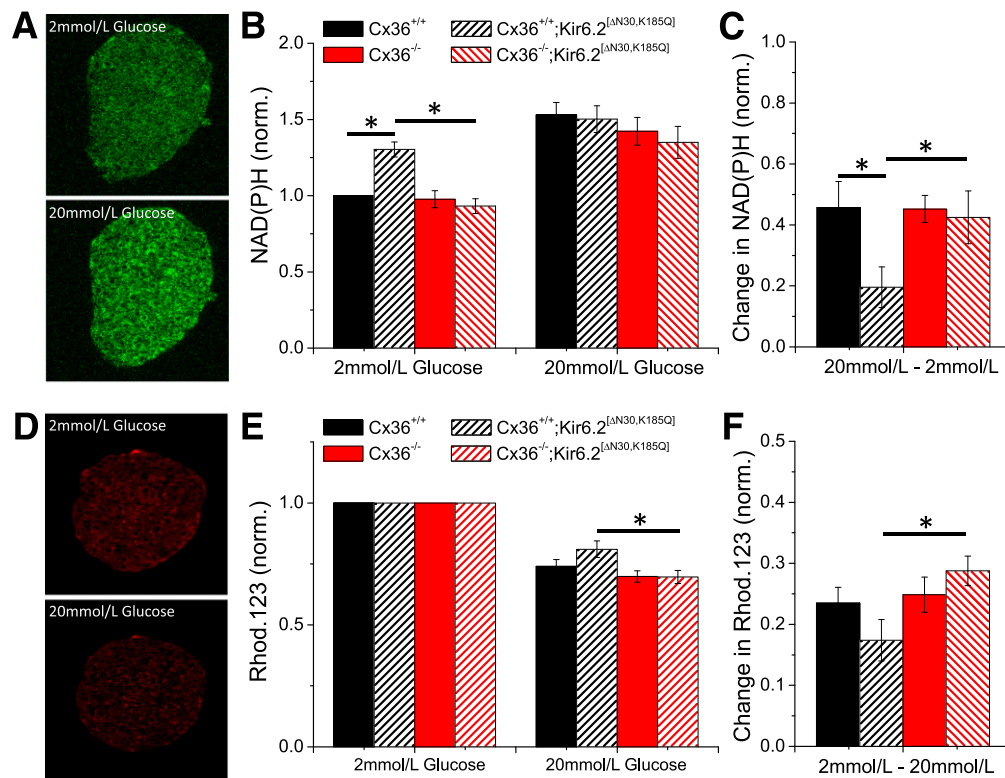
Figure 6—Prevention of secondary mitochondrial defects. A: Representative NAD(P)H autofluorescence image at 2 mmol/L glucose (top) and 20 mmol/L glucose (bottom) in a $Cx36^{+/+}$ islet. B: Mean NAD(P)H autofluorescence in islets isolated from $Cx36^{+/+};Kir6.2^{[\Delta N30,K185Q]}$ and $Cx36^{+/+}$ littermate control mice and $Cx36^{-/-};Kir6.2^{[\Delta N30,K185Q]}$ and $Cx36^{-/-}$ littermate control mice. Data are normalized (norm.) to mean NAD(P)H fluorescence measured in $Cx36^{+/+}$ islets at 2 mmol/L glucose. C: Change in NAD(P)H from 2 to 20 mmol/L glucose in islets from each experimental group in B. Data in A and B averaged over $n = 5$ age-matched mice in each group, two to four islets per mouse. D: Representative Rhodamine 123 fluorescence image at 2 (top) and 20 mmol/L glucose (bottom) in a $Cx36^{+/+}$ islet. E: Mean Rhodamine 123 fluorescence in islets isolated from $Cx36^{+/+};Kir6.2^{[\Delta N30,K185Q]}$ and $Cx36^{+/+}$ littermate control mice and $Cx36^{-/-};Kir6.2^{[\Delta N30,K185Q]}$ and $Cx36^{-/-}$ littermate control mice. Data are normalized to fluorescence at 2 mmol/L glucose in each experimental group. F: Change in Rhodamine 123 fluorescence from 2 to 20 mmol/L glucose in islets from each experimental group in E. Data in E and F averaged over $n = 5$ age-matched mice in each group, two to six islets per mouse. *Significant difference ($P < 0.05$, two-tailed Student t test) between each experimental group as indicated. Error bars represent mean ± SEM.

junction–mediated current. This suppresses $[Ca^{2+}]_i$ elevations and insulin release across the islet. In the absence of Cx36 gap junction coupling, this current is absent (17) and therefore normally excitable cells are free to depolarize, elevate $[Ca^{2+}]_i$, and release insulin at elevated glucose levels.

Gap Junction Suppression of $[Ca^{2+}]_i$ Is Physiologically Important

Previous work has shown that membrane depolarization and $[Ca^{2+}]_i$ elevations in excitable cells of an islet can be suppressed by gap junction coupling to inexcitable cells. This was demonstrated in islets expressing a K_{ATP} loss-of-function mutation (closes in the absence of ATP) at low (~2 mmol/L) glucose (16), where a reduction of gap junction coupling elevated $[Ca^{2+}]_i$. Similar observations have been made in normal islets at basal (~5 mmol/L) glucose (17,18). Here, in the presence overactive ATP-insensitive K_{ATP} channels (Fig. 4), or diazoxide-induced K_{ATP} channel opening (Fig. 5), a reduction of gap junction

coupling also elevated $[Ca^{2+}]_i$. This shows that a general principle exists whereby gap junction channel closure/deletion can (at least partially) counteract the effect of K_{ATP} channel opening to elevate $[Ca^{2+}]_i$.

Importantly, in the presence of a gain-of-function mutation to the K_{ATP} channels, there was no elevation in $[Ca^{2+}]$ and insulin release at lower glucose levels. As described above, likely a reduction in Cx36 imparts a left shift to the glucose-stimulated $[Ca^{2+}]_i$ response rather than a constitutive elevation, counteracting the right shift after ATP-insensitive mutant K_{ATP} channel expression. Thus, a reduction in Cx36 cannot counteract the very strong K_{ATP} opening that results from low glucose and ATP-insensitive K_{ATP} channels. This suggests that a Cx36 gap junction reduction would be unlikely to counteract very strong mutations to the K_{ATP} channel, as is also suggested by very high diazoxide treatment (Fig. 5).

Interestingly, in islets from $Cx36^{-/-};Kir6.2^{[\Delta N30,K185Q]}$ mice, even those high-GFP+ cells that were inexcitable in
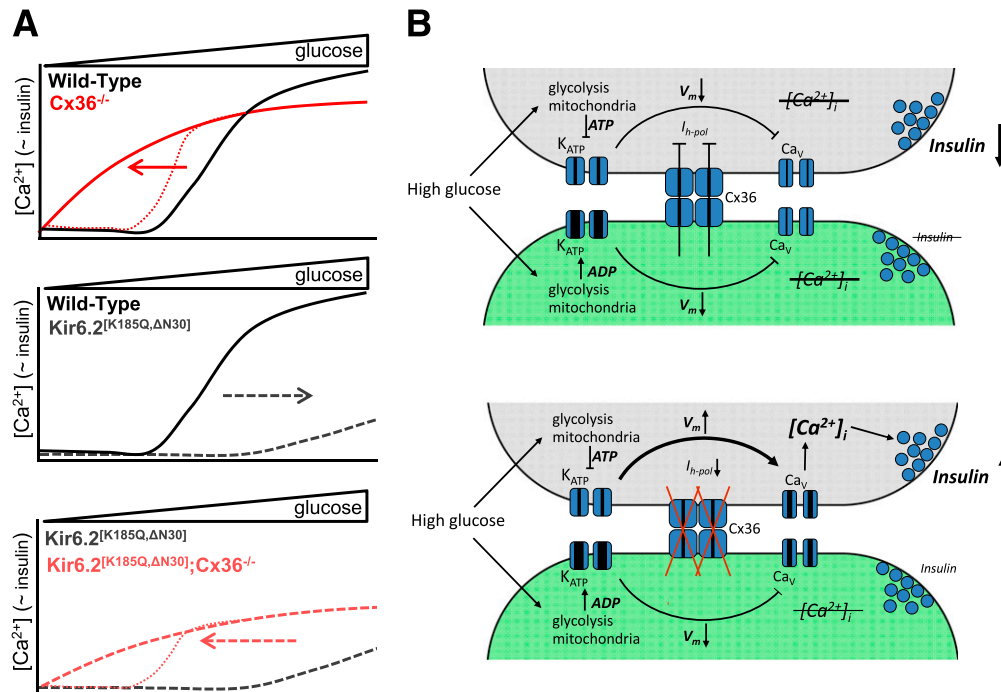
Figure 7—Schematic describing recovery of insulin secretion. *A*: Schematic representation for glucose-stimulated $[Ca^{2+}]_i$ as a result of changes to Cx36 and K_{ATP} activity. *Top*: Reduction in Cx36 activity due to genetic knockout leads to a left shift and more gradual dose response of $[Ca^{2+}]_i$ (solid red). Disrupted dynamics not shown. Note insulin at low glucose is still suppressed due to action of another communication mechanism (dotted red). *Middle*: Increase in K_{ATP} activity due to mutations that reduce the sensitivity of ATP inhibition leads to a right shift in dose response in $[Ca^{2+}]_i$ (dashed black), such that it is largely suppressed within experimental glucose ranges. Insulin follows this dose response. *Bottom*: In the presence of increased K_{ATP} activity, a reduction in Cx36 activity leads to a left shift in the dose response of $[Ca^{2+}]_i$ back to within a physiological range (dashed red), albeit with glucose-stimulated activity slightly blunted compared with a reduction in Cx36 activity alone. Insulin follows this dose response, although at low glucose it is still suppressed due to action of another communication mechanism (dotted red). *B*: Two representative, neighboring cells in an islet, with one inexcitable cell (intrinsically inexcitable or expressing high levels of ATP-insensitive K_{ATP} channels: *lower*, green) and one excitable cell (with near-normal K_{ATP} channels: *upper*, gray). At elevated glucose, the inexcitable cell remains hyperpolarized (V_m low). In isolation, the excitable cell would depolarize (V_m increase), elevate $[Ca^{2+}]_i$, and release insulin. However, Cx36 gap junction coupling mediates a hyperpolarizing current (I_{h-pol}) from the inexcitable cell to the excitable cell, preventing depolarization and $[Ca^{2+}]_i$ elevations, thereby suppressing Ca^{2+} triggering of insulin secretion across the islet. In the absence of Cx36 gap junction coupling, the hyperpolarizing current is abolished and the more excitable cell depolarizes and elevates $[Ca^{2+}]_i$, which triggers insulin secretion.

the presence of gap junctions showed some $[Ca^{2+}]_i$ elevations. These were less frequent than in the more excitable low-GFP⁻ cells but significantly more than in islets of Cx36$^{+/+}$;Kir6.2$^{[ΔN30,K185Q]}$ mice (Fig. 4). Electrically uncoupled cells will likely show some stochastic "channel noise," as suggested by modeling studies (23,24), which may be sufficient to transiently depolarize and elevate $[Ca^{2+}]_i$. This suggests that electrically uncoupled cells may inherently behave different to β-cells in normal islets, warranting further study.

Importantly, the elevated $[Ca^{2+}]_i$ at elevated glucose levels that follows a reduction of gap junction coupling also led to elevated insulin secretion (Figs. 3 and 5). This contrasts with the behavior at lower glucose levels in normal islets (18), where this effect is normally masked due to other mechanisms of cell-cell communication that suppress insulin release independent of $[Ca^{2+}]_i$. However, it was suggested that this other communication mechanism(s) that suppresses insulin

is inactive at elevated glucose (18,25), as we have demonstrated.

Of further importance, the gap junction–mediated suppression of islet $[Ca^{2+}]_i$ and insulin release is physiologically important. By eliminating gap junction coupling in mice expressing ATP-insensitive K_{ATP} channels, we eliminated hyperglycemia (Fig. 1). Gap junction coupling in the islet has been shown to play an important physiological role: to coordinate and enhance the first phase of insulin secretion and coordinate the pulsatile second phase of insulin secretion (15). In its absence, glucose intolerance occurs, and we observed glucose intolerance in Cx36$^{-/-}$;Kir6.2$^{[ΔN30,K185Q]}$ mice, albeit slightly less than previously observed (15), likely due to the younger age of the mice. This physiological role gives a new fundamental understanding of the multicellular properties of the islet, specifically how the electrical coupling of β-cells via gap junction channels can be critically important to coordinate K_{ATP} channel–regulated

electrical activity to regulate insulin secretion and glucose homeostasis.

Relevance to Human NDM

The majority of cases of NDM (~60%) occur as a result of gain-of-function mutations to the Kir6.2 or Sur1 subunits of the K_{ATP} channel (26). In the normal presence of Cx36, we observed similar results to a prior mouse model that expresses a Kir6.2 mutation associated with NDM (4), including marked hyperglycemia, reduced weight gain, reduced islet insulin content, and suppression of glucose-stimulated $[Ca^{2+}]_i$ and insulin. Despite the reduced insulin content, normal depolarization-induced $[Ca^{2+}]_i$ and insulin release was observed, also as previously observed (4). Given that a reduction of Cx36 gap junction coupling so dramatically normalized glycemic control, we anticipate an improvement in islet function would occur in humans with NDM. However, some subtle differences must be discussed.

The distribution of Kir6.2$^{[\Delta N30, K185Q]}$ expression is likely more heterogeneous in islets from this mouse model compared with islets of humans with the disease, due to the stochastic and variable nature of Pdx-Cre^{ER}–mediated recombination (21). Therefore, the heterogeneity in β-cell function, from which the gap junction–mediated suppression of $[Ca^{2+}]_i$ and insulin partly occurs, will not be exactly the same. However, it is well established that human and mouse β-cells lacking cellular proximity are very heterogeneous in their glucose response (27,28). This suggests that a Cx36 gap junction reduction will elevate glucose-stimulated $[Ca^{2+}]_i$ and insulin even in the presence of uniform Kir6.2$^{[\Delta N30, K185Q]}$ expression. Results from diazoxide-treated islets (Fig. 5) support this, as diazoxide treatment likely provides uniform K_{ATP} opening across the islet. In this case, the endogenous β-cell heterogeneity would be closer to that of human islets with NDM mutations. Further, gap junction coupling suppresses excitability in other conditions of K_{ATP} channel opening at lower glucose levels. In Cx36$^{-/-}$ islets, elevated $[Ca^{2+}]_i$ is observed in ~50% of β-cells at 5 mmol/L glucose (18), and in ~40% of β-cells upon 100 μmol/L diazoxide (Fig. 5), each similar to that after expression of Kir6.2$^{[\Delta N30, K185Q]}$ (Fig. 4). The precise quantitative balance between β-cell heterogeneity and gap junction coupling in determining islet function remains to be determined. Nevertheless, the presence of any heterogeneity will lead to gap junction coupling suppressing $[Ca^{2+}]_i$ over a certain range of glucose levels. Likely, the broader the heterogeneity, the greater the difference in the presence and absence of gap junction coupling (18) and the more dramatic the effect in modulating gap junction coupling.

The discovery that NDM can be caused by gain-of-function mutations to the Kir6.2 and Sur1 subunits of the K_{ATP} channel has meant that patients can switch from insulin therapy to oral sulfonylurea treatment with improved glycemic control (7). Although successful for treating NDM, sulfonylurea treatment has been reported to be associated with hypoglycemic episodes (29), which may occur due to constitutive glucose-independent K_{ATP} channel closure, which reduces the low glucose regulation of insulin secretion. Chronic sulfonylurea therapy can also cause glucose intolerance (30), possibly resulting from overstimulation of $[Ca^{2+}]_i$. As discussed above, a modulation of gap junction coupling retains a suppression of $[Ca^{2+}]_i$ and insulin secretion at low glucose (Figs. 3, 4, and 7) and thus would be anticipated to lessen potential hypoglycemia. More importantly, some Kir6.2 and Sur1 mutations reduce the sensitivity of sulfonylurea inhibition (7,9,10), reducing sulfonylurea effectiveness. We speculate that modulating Cx36 gap junction coupling may provide an alternative route to elevate glucose-stimulated $[Ca^{2+}]_i$ and insulin secretion, particularly in the presence of sulfonylurea-insensitive mutations.

Here, a near-complete reduction in gap junction coupling (>95%, Cx36$^{-/-}$) normalized blood glucose levels, but a partial reduction (~50%, Cx36$^{+/-}$) had a minimal effect (Supplementary Fig. 1). This Cx36 dose response is similar to how reducing Cx36 gap junction coupling disrupts glucose tolerance via first-phase and second-phase insulin dynamics (15). As a potential therapeutic target, we therefore anticipate that a gap junction inhibition of >50% would be required. Current inhibitors are weak with nonspecific effects, although a recent study developed a novel screen for gap junction modulators (31), which may yield more potent and specific inhibitors. A partial disruption to gap junction coupling can also result from hyperglycemia (32). However, in Cx36$^{+/+}$; Kir6.2$^{[\Delta N30, K185Q]}$ islets, significant coupling is still present, as shown by the coordinated residual $[Ca^{2+}]_i$. Therefore, any Cx36 decrease resulting from hyperglycemia would likely be insufficient to significantly alter insulin release in this model.

In principle, we anticipate that reducing gap junction coupling could similarly correct defects in insulin release caused by mutations proximal to $[Ca^{2+}]_i$ influx, including glucokinase (33,34) and genes that regulate mitochondrial function (35,36). Defects in proximal steps could affect the "amplifying" pathways that regulate insulin release (37), and reduce the effect of gap junction modulation. However, altering the K_{ATP} regulation of membrane potential can compensate for an absence of glucokinase (38). Therefore, modulating Cx36 gap junction coupling may be more broadly applicable to normalize islet function.

To summarize, we have shown that by reducing gap junction coupling between β-cells in a model of NDM caused by expression of ATP-insensitive K_{ATP} channels, we can eliminate severe hyperglycemia and islet dysfunction. This is achieved through a novel pathway where a reduction in Cx36 can partially

compensate for overactive K_{ATP} channels and prevent suppression of electrical activity across the islet. This restores glucose-stimulated $[Ca^{2+}]_i$, insulin secretion, and glucose homeostasis. This yields a better understanding of how the islet functions as a coupled unit of β-cells and may ultimately provide a potential therapeutic target for treating NDM and other monogenic forms of diabetes.

References

1. Nichols CG. KATP channels as molecular sensors of cellular metabolism. Nature 2006;440:470–476

2. Gloyn AL, Pearson ER, Antcliff JF, et al. Activating mutations in the gene encoding the ATP-sensitive potassium-channel subunit Kir6.2 and permanent neonatal diabetes. N Engl J Med 2004;350:1838–1849

3. Remedi MS, Kurata HT, Scott A, et al. Secondary consequences of beta cell inexcitability: identification and prevention in a murine model of K(ATP)-induced neonatal diabetes mellitus. Cell Metab 2009;9:140–151

4. Girard CA, Wunderlich FT, Shimomura K, et al. Expression of an activating mutation in the gene encoding the KATP channel subunit Kir6.2 in mouse pancreatic beta cells recapitulates neonatal diabetes. J Clin Invest 2009;119:80–90

5. Koster JC, Marshall BA, Ensor N, Corbett JA, Nichols CG. Targeted over-activity of beta cell K(ATP) channels induces profound neonatal diabetes. Cell 2000;100:645–654

6. Benninger RKP, Remedi MS, Head WS, Ustione A, Piston DW, Nichols CG. Defects in beta cell Ca²+ signalling, glucose metabolism and insulin secretion in a murine model of K(ATP) channel-induced neonatal diabetes mellitus. Diabetologia 2011;54:1087–1097

7. Pearson ER, Flechtner I, Njølstad PR, et al.; Neonatal Diabetes International Collaborative Group. Switching from insulin to oral sulfonylureas in patients with diabetes due to Kir6.2 mutations. N Engl J Med 2006;355:467–477

8. Wambach JA, Marshall BA, Koster JC, White NH, Nichols CG. Successful sulfonylurea treatment of an insulin-naïve neonate with diabetes mellitus due to a KCNJ11 mutation. Pediatr Diabetes 2010;11:286–288

9. Proks P, Antcliff JF, Lippiat J, Gloyn AL, Hattersley AT, Ashcroft FM. Molecular basis of Kir6.2 mutations associated with neonatal diabetes or neonatal diabetes plus neurological features. Proc Natl Acad Sci USA 2004;101:17539–17544

10. Koster JC, Remedi MS, Dao C, Nichols CG. ATP and sulfonylurea sensitivity of mutant ATP-sensitive K+ channels in neonatal diabetes: implications for pharmacogenomic therapy. Diabetes 2005;54:2645–2654

11. Lernmark A. The preparation of, and studies on, free cell suspensions from mouse pancreatic islets. Diabetologia 1974;10:431–438

12. Zhang M, Goforth P, Bertram R, Sherman A, Satin L. The Ca2+ dynamics of isolated mouse beta-cells and islets: implications for mathematical models. Biophys J 2003;84:2852–2870

13. Benninger RKP, Zhang M, Head WS, Satin LS, Piston DW. Gap junction coupling and calcium waves in the pancreatic islet. Biophys J 2008;95:5048–5061

14. Ravier MA, Güldenagel M, Charollais A, et al. Loss of connexin36 channels alters beta-cell coupling, islet synchronization of glucose-induced Ca2+ and insulin oscillations, and basal insulin release. Diabetes 2005;54:1798–1807

15. Head WS, Orseth ML, Nunemaker CS, Satin LS, Piston DW, Benninger RKP. Connexin-36 gap junctions regulate in vivo first- and second-phase insulin secretion dynamics and glucose tolerance in the conscious mouse. Diabetes 2012;61:1700–1707

16. Rocheleau JV, Remedi MS, Granada B, et al. Critical role of gap junction coupled KATP channel activity for regulated insulin secretion. PLoS Biol 2006;4:e26

17. Speier S, Gjinovci A, Charollais A, Meda P, Rupnik M. Cx36-mediated coupling reduces beta-cell heterogeneity, confines the stimulating glucose concentration range, and affects insulin release kinetics. Diabetes 2007;56:1078–1086

18. Benninger RKP, Head WS, Zhang M, Satin LS, Piston DW. Gap junctions and other mechanisms of cell-cell communication regulate basal insulin secretion in the pancreatic islet. J Physiol 2011;589:5453–5466

19. Pipeleers DG. Heterogeneity in pancreatic beta-cell population. Diabetes 1992;41:777–781

20. Degen J, Meier C, Van Der Giessen RS, et al. Expression pattern of lacZ reporter gene representing connexin36 in transgenic mice. J Comp Neurol 2004;473:511–525

21. Zhang HJ, Fujitani Y, Wright CVE, Gannon M. Efficient recombination in pancreatic islets by a tamoxifen-inducible Cre-recombinase. Genesis 2005;42:210–217

22. Hraha TH, Bernard AB, Nguyen LM, Anseth KS, Benninger RKP. Dimensionality and size scaling of coordinated Ca2+ dynamics in MIN6 β-cell clusters. Biophys J 2014;106:299–309

23. Jo J, Kang H, Choi MY, Koh DS. How noise and coupling induce bursting action potentials in pancreatic beta-cells. Biophys J 2005;89:1534–1542

24. Bertram R, Sherman A. Dynamical complexity and temporal plasticity in pancreatic beta-cells. J Biosci 2000;25:197–209

25. Konstantinova I, Nikolova G, Ohara-Imaizumi M, et al. EphA-Ephrin-A-mediated beta cell communication regulates insulin secretion from pancreatic islets. Cell 2007;129:359–370

26. Hattersley AT, Ashcroft FM. Activating mutations in Kir6.2 and neonatal diabetes: new clinical syndromes, new scientific insights, and new therapy. Diabetes 2005;54:2503–2513

27. Van Schravendijk CF, Kiekens R, Pipeleers DG. Pancreatic beta cell heterogeneity in glucose-induced insulin secretion. J Biol Chem 1992;267:21344–21348

28. Wojtusciszyn A, Armanet M, Morel P, Berney T, Bosco D. Insulin secretion from human beta cells is heterogeneous and dependent on cell-to-cell contacts. Diabetologia 2008;51:1843–1852

29. Codner E, Flanagan SE, Ugarte F, et al. Sulfonylurea treatment in young children with neonatal diabetes: dealing with hyperglycemia, hypoglycemia, and sick days. Diabetes Care 2007;30:e28–e29

30. Remedi MS, Nichols CG. Chronic antidiabetic sulfonylureas in vivo: reversible effects on mouse pancreatic beta-cells. PLoS Med 2008;5:e206

31. Bavamian S, Pontes H, Cancela J, et al. The intercellular synchronization of Ca2+ oscillations evaluates Cx36-dependent coupling. PLoS ONE 2012;7:e41535

32. Carvalho CP, Oliveira RB, Britan A, et al. Impaired β-cell–β-cell coupling mediated by Cx36 gap junctions in prediabetic mice. Am J Physiol Endocrinol Metab 2012;303:E144–E151

33. Njølstad PR, Søvik O, Cuesta-Muñoz A, et al. Neonatal diabetes mellitus due to complete glucokinase deficiency. N Engl J Med 2001;344:1588–1592

34. Vionnet N, Stoffel M, Takeda J, et al. Nonsense mutation in the glucokinase gene causes early-onset non-insulin-dependent diabetes mellitus. Nature 1992;356:721–722

35. Yamagata K, Furuta H, Oda N, et al. Mutations in the hepatocyte nuclear factor-4alpha gene in maturity-onset diabetes of the young (MODY1). Nature 1996;384:458–460

36. Wang H, Maechler P, Hagenfeldt KA, Wollheim CB. Dominant-negative suppression of HNF-1alpha function results in defective insulin gene transcription and impaired metabolism-secretion coupling in a pancreatic beta-cell line. EMBO J 1998;17:6701–6713

37. Henquin JC. Triggering and amplifying pathways of regulation of insulin secretion by glucose. Diabetes 2000;49:1751–1760

38. Remedi MS, Koster JC, Patton BL, Nichols CG. ATP-sensitive K+ channel signaling in glucokinase-deficient diabetes. Diabetes 2005;54:2925–2931